Predicting a new Phase (T") of two-dimensional Transition Metal Di-Chalcogenides and Strain-controlled Topological Phase Transition

Fengxian Ma[1], Guoping Gao[1], Yalong Jiao[1], Yuantong Gu[1], Ante Bilic[2], Haijun Zhang[3], Zhongfang Chen[3] and Aijun Du[1,]*

[1]School of Chemistry, Physics and Mechanical Engineering Faculty, Queensland University of Technology, Garden Point Campus, QLD 4001, Brisbane, Australia

[2]CSIRO Manufacturing, Virtual Nanoscience Lab, Parkville 3052 VIC, Australia

[3]Department of Chemistry, University of Puerto Rico, Rio Piedras Campus, San Juan, Puerto Rico 00931, United States

Method

We employed the swarm-intelligence based CALYPSO method [1,2] for the global structure search. Effectiveness of CALYPSO method has been demonstrated by the recent successful applications in predicting crystal structure in a diverse range of 3D materials [3,4] and 2D structures. [5-8]. Structure searches for MoS_2 with simulation cells ranging from one to six formula units were performed at zero GPa. Each generation contained 30 structures, and initial structures in the first generation were produced randomly with symmetry constraints. All the structures are optimized to their local minima by using DFT (VASP code) [9] calculations. During structure evolution, 60% of structures in the first generation with lower enthalpies are selected to produce the structures in the next generation by PSO. 40% of the structures in the new generation are randomly generated. The local optimizations are performed using the conjugate gradients method and the converging criteria of the enthalpy change in convective SCF steps is $1x10^{-4}$ eV per atom. We find that the simulations successfully reproduce all the previously reported 2H-MoS_2, 1T-MoS_2, 1T'-MoS_2 structural phases and the new mix-phase T" in the first five generations. After that *ab initio* structural relaxation and electronic band-structure calculations were carried out using density functional theory (DFT) with the Perdew-Burke-Ernzerhof (PBE) generalized gradient approximation [10] exchange-correlation potential as implemented in the Vienna Ab initio simulation package (VASP). [9,11] A dispersion correction of the total energy (DFT-D3 method) [12] was used to incorporate the long-range van der Waals interaction. An energy cut-off of 400 eV for the plane-wave expansion and Monkhorst-Pack k-point meshes of 5 × 17 × 1 and 5 × 21 × 1 in the 2D Brillouin zone (BZ) were used for the geometry optimization of new mixed T" MoS_2 structural phase and electronic structure calculation. During the geometry optimization, the atomic position and lattice vectors were fully relaxed until energy and force were converged to 10^{-5} eV and 0.002 eV/Å, respectively. It is well known that the PBE functional typically underestimates the energy band gap. So the state-of-the-art hybrid functional (HSE06) [13] is carried out for comparison. To make sure of the

dynamical stability of the obtained structures, phonon dispersion analysis was performed by the finite displacement method [14] using the Phonopy code [15] interfaced with the density functional perturbation theory [16] as implemented in VASP. In phonon calculations, an increased plane wave energy cut-off of 500 eV were employed, accompanied with more stringent convergence criteria.

T" phase of MoS_2 Space group (No.6) PM	a=11.23 Å b=3.16 Å c=25.6 Å	Mo 0.64946 0.50000 0.49082 Mo 0.15922 0.50000 0.45956 Mo 0.40297 0.00000 0.47710 Mo 0.84159 -0.00000 0.47404 S 0.77214 0.50000 0.41277 S 0.50296 0.50000 0.42211 S 0.98096 0.50000 0.52047 S 0.46534 0.50000 0.54281 S 0.21892 -0.00000 0.52642 S 0.26577 -0.00000 0.40465 S 0.01964 -0.00000 0.41748 S 0.72101 0.00000 0.55181

Table S1. The crystallographic information (space group, optimized lattice parameters, and occupied lattice sites (fractional coordinates) of the hybrid T" MoS_2 phase.

To further understand the phase transition between topological phase and trivial insulator phase with the increasing strain, we calculate density of orbit state of T" mix MoS_2 under different strain as shown in fig. S1 (a-c). As shown in fig. S1 (a), the valence band mainly consists of d_{z2} and d_{xz} orbitals of Mo atoms and p_z of S, while the conduction band mainly consists of d_{xy} orbitals of Mo atoms and p_y of S at 0% strain. At the point of 2% strain, the d-orbit and p-orbit touch each other at Fermi level (0 eV) position, forming a critical point of phase transition between topological phase and trivial insulator phase. For larger values of strain, the d-orbit and p-orbit separate in an opposite direction again with an exchange of orbit. For example, the valence band mainly consists of d_{xy} orbitals of Mo atoms and p_y of S, while the conduction band mainly consists of d_{z2} and d_{xz} orbitals of Mo atoms and pz of S at 3% strain (fig. S1 (c)). All these changes of DOS under strain are consisted with the process of band gap closing to reopen, and with the exchange of HOMO and LUMO.

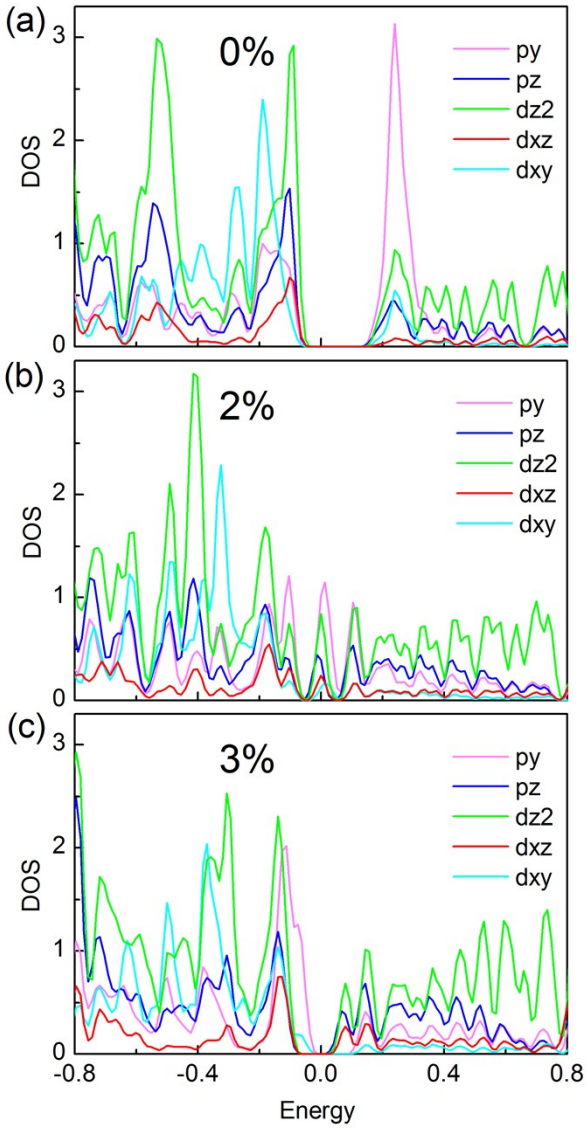

Fig. S1. Density of states (DOS) of T" MoS_2 phase under different strain (a) 0%, (b) 2%, (c) 3%.

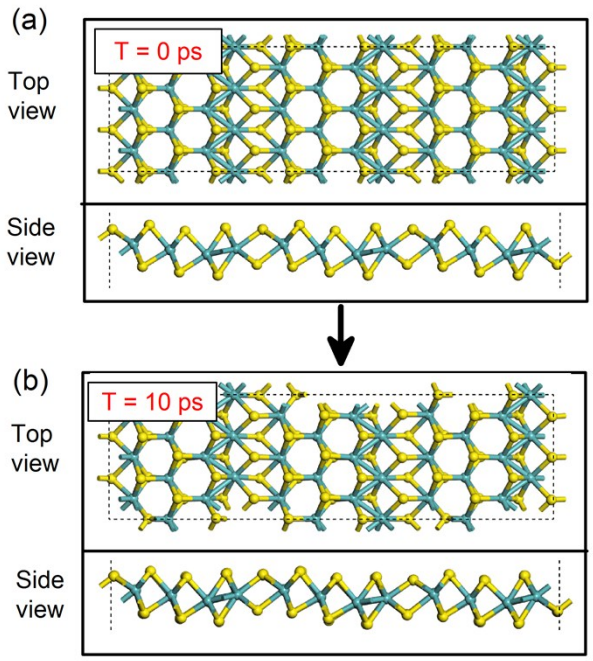

Fig. S2. Top and side view of T" MoS_2 at (a) 0 ps and (b) 10 ps in the MD simulation.

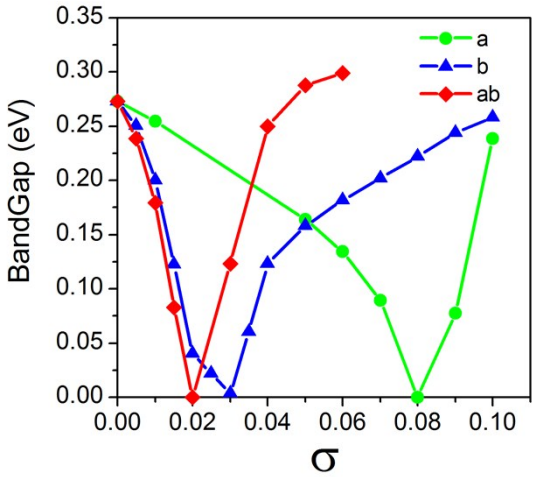

Fig. S3. The band gap as a function of uniaxial a-axis (green line), b-axis (blue line) and biaxial (red line) strain for the T" MoS_2 phase.

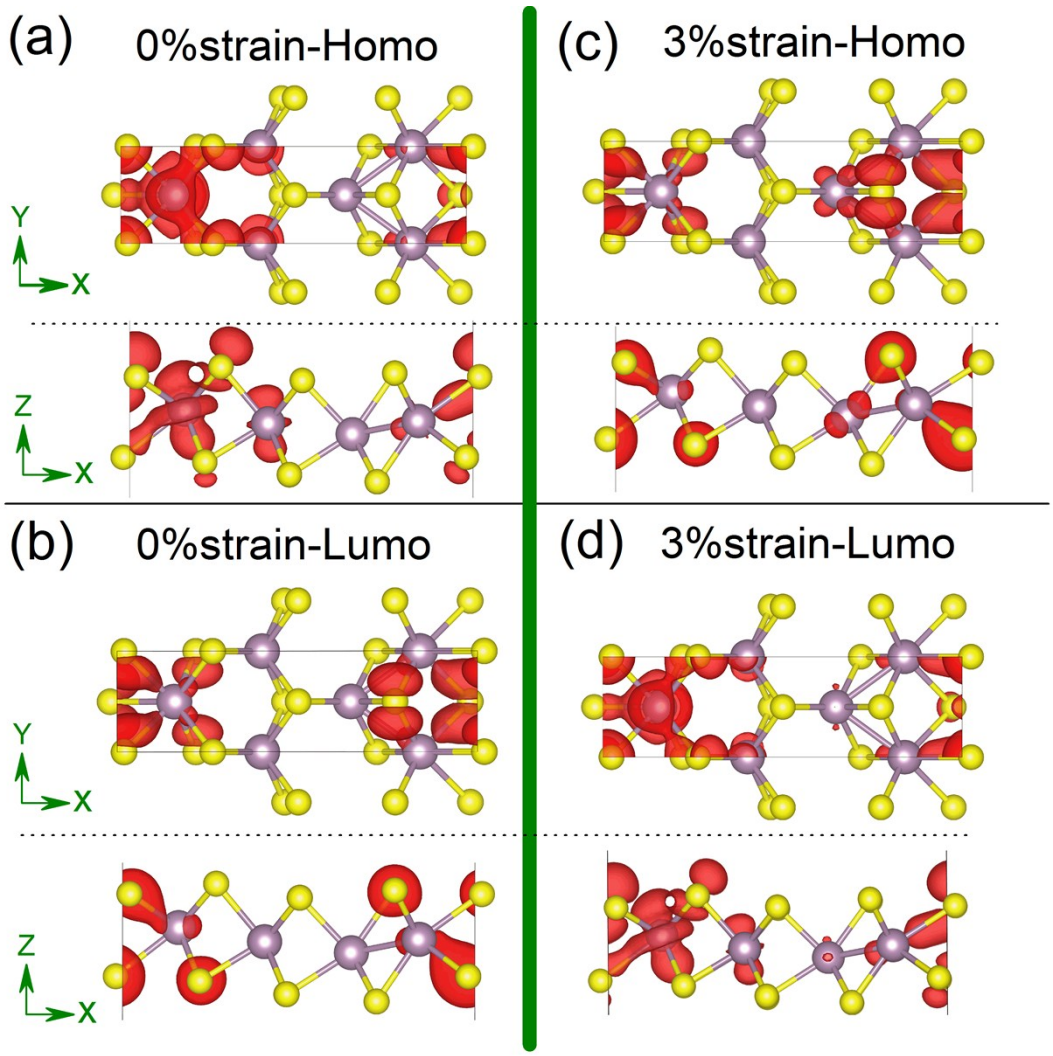

Fig. S4. Orbital density distributions at the VB and CB edges of the T" MoS_2 hybrid phase under different strains 0% (a-b) and 3% (c-d).

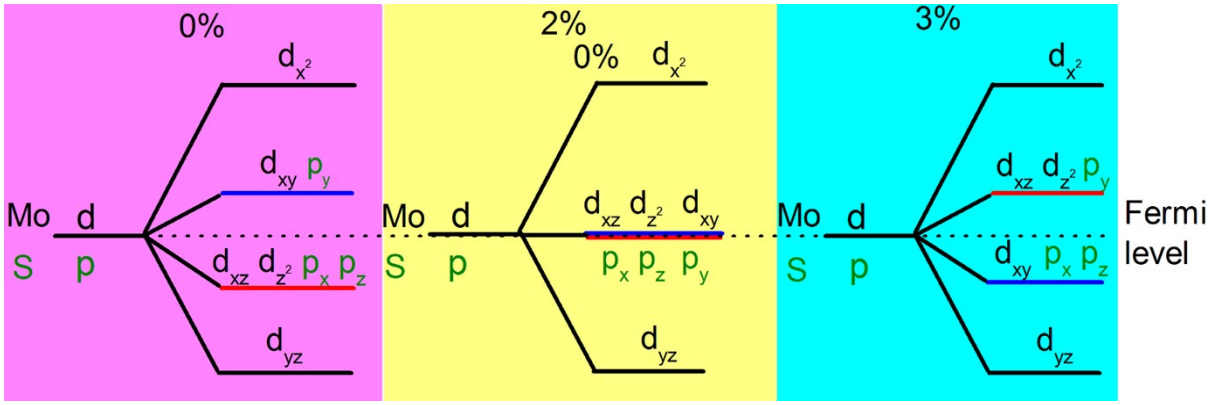

Fig. S5. Orbital energy of T” MoS_2 under different strains.

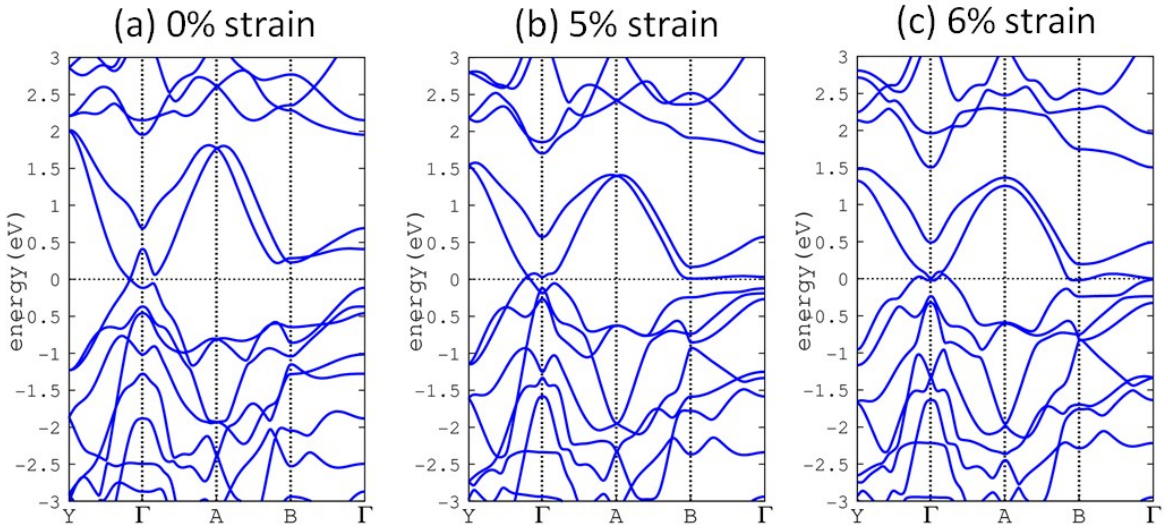

Fig. S6 The band structure of 1T' MoS_2 under biaxial strain.

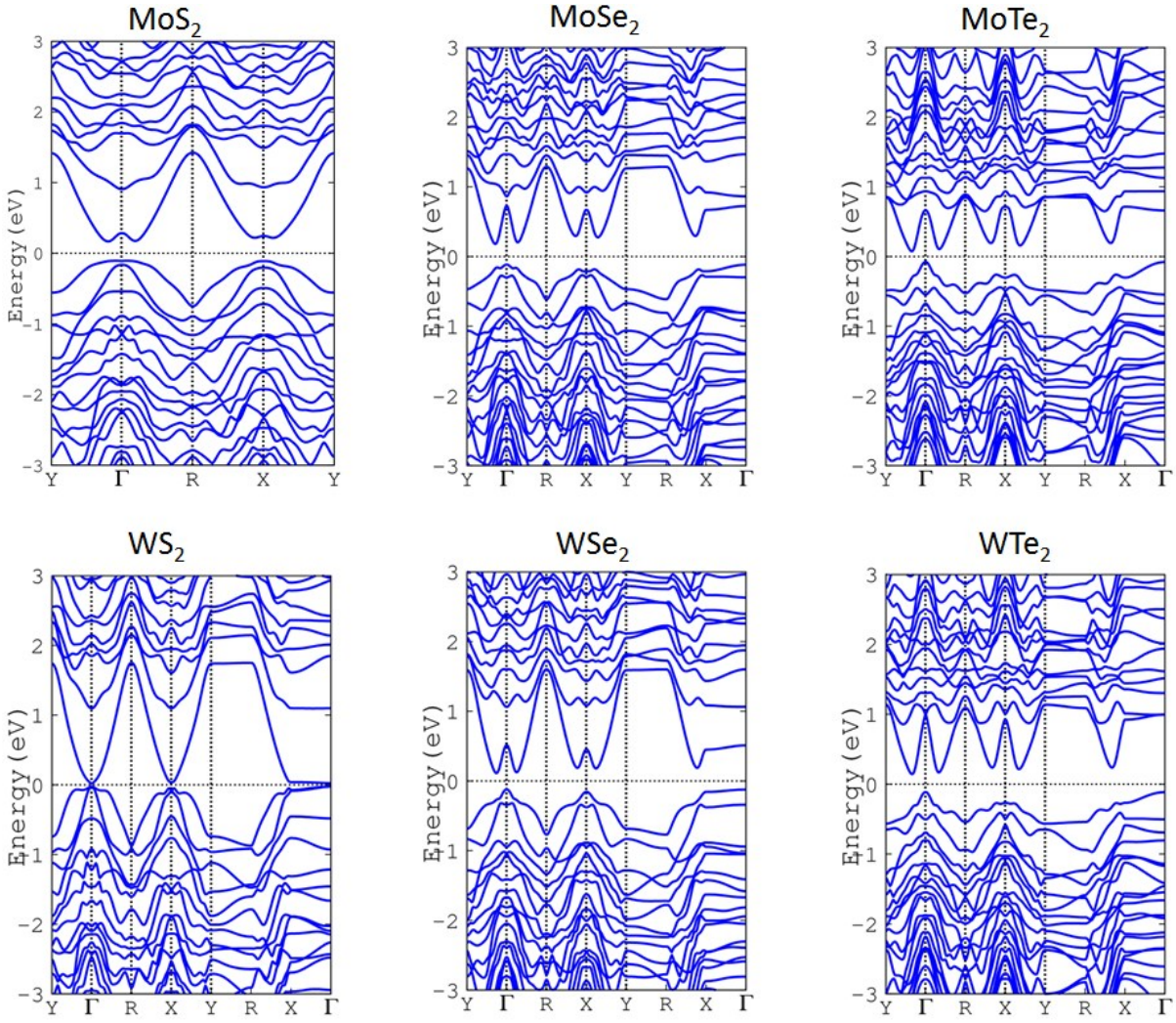

Fig. S7. Electronic band structure of monolayer transition metal dichalcogenides T"-MX2 (MoS_2, $MoSe_2$, $MoTe_2$, WS_2, WSe_2 and WTe_2).

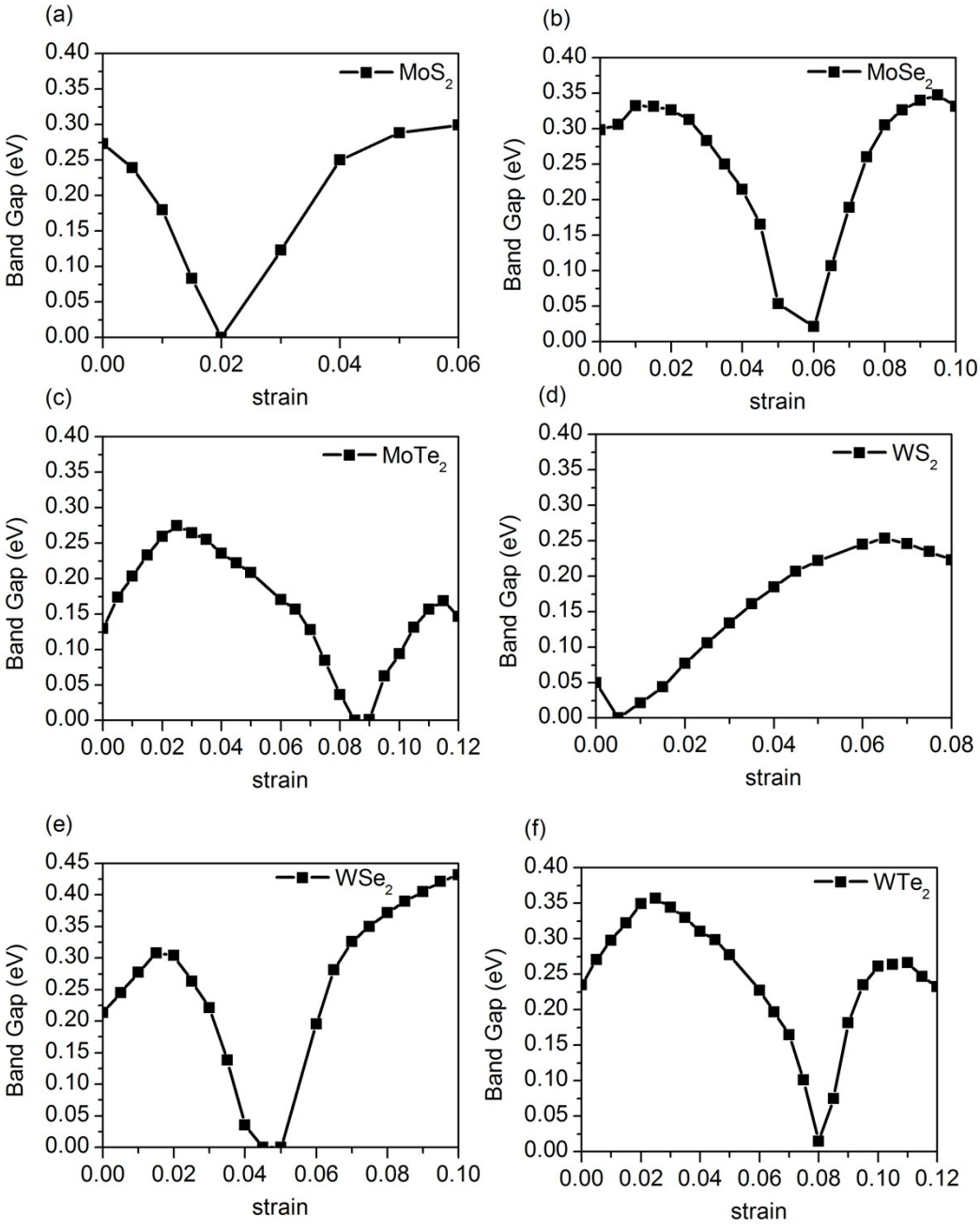

Fig. S8. The band gap as a function of biaxial strain of of monolayer transition metal dichalcogenides T”-MX2 (MoS_2, $MoSe_2$, $MoTe_2$, WS_2, WSe_2 and WTe_2).

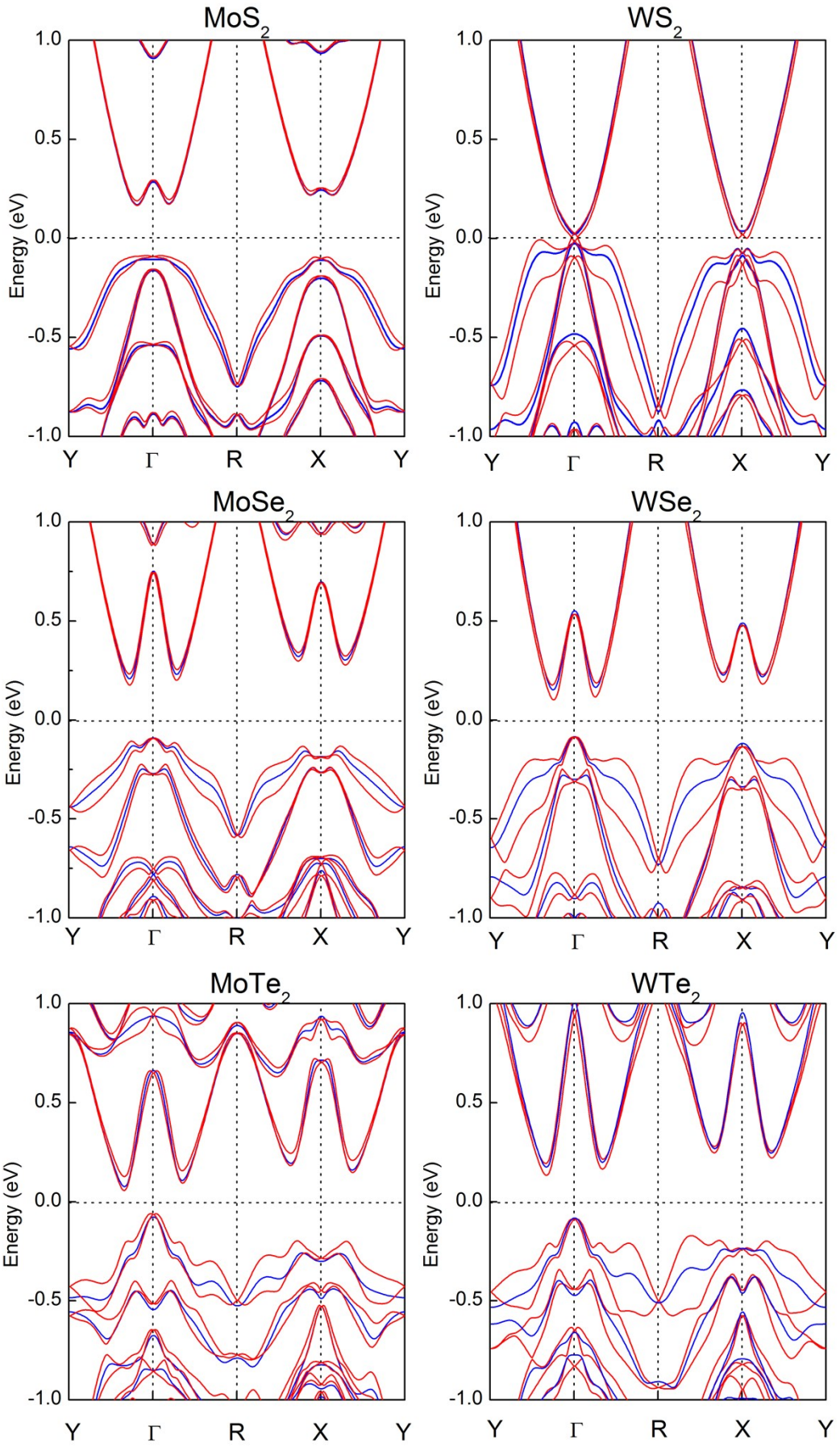
MoS2
WS2
MoSe2
WSe2
MoTe2
WTe2
Energy (eV)
1.0
0.5
0.0
-0.5
-1.0
Y
Γ
R
X
Y

Fig. S9. Electronic band structure of monolayer transition metal dichalcogenides T”-MX2 with (red line) and without (blue line) spin-orbit coupling. The calculations were performed by first-principles density functional theory with the PBE exchange-correlation functional.

The topologically protected conducting edge state inside the bulk band gap is the hallmark of 2D topological insulators. Therefore, in order to further confirm the topological nontrivial nature of T” MoS_2, we have checked the existence of protected gapless edge states. A MoS_2 nanoribbon with zigzag edges is considered, as shown in Fig. S8 (b, c). For the zigzag nanoribbon, the termination of two sides keep T’ partial because of the significant contribution of T’ part in the T” structure. The width of the nanoribbon (7.3 nm) is large enough to avoid interactions between the edge states of the two sides. The band structure of the nanoribbon is shown in Figure S8 (a). The contribution from the top edge is marked with red line, while that from the bottom edge is marked with blue line. We can see explicitly that the gapless edge states appear in bulk gap. In addition the real space orbital density distributions of the edge states of the system at the whole Brillouin zone are depicted in Fig. S8 (b, c). We can observe that the topologically protected edge states derive from the ribbon edges. All these confirmed the topological nontrivial property of mixed T” MoS_2.

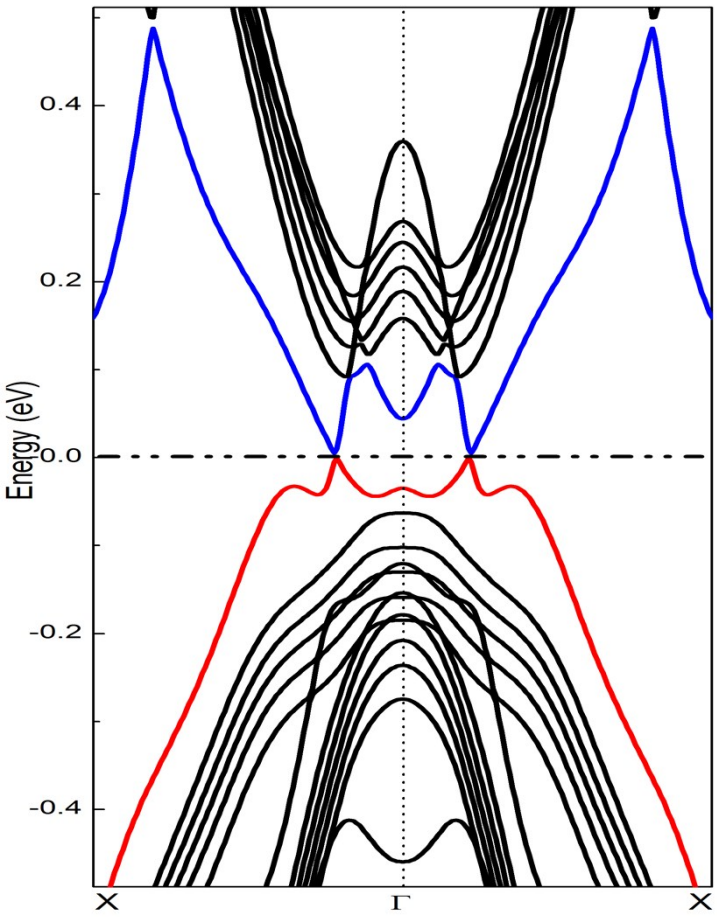

Fig. S10. Electronic band structure of T” MoS_2 nanoribbon with length (L) 7.3 nm (a); The orbital density distributions of the gapless edge states can be clearly seen on the edges of the nanoribbon: the blue one represents the Lomo (b), and the red indicates the Homo (c).

Reference

[1] Y. Wang, J. Lv, L. Zhu, and Y. Ma, Comput. Phys. Commun. **183**, 2063 (2012).
[2] Y. Wang, J. Lv, L. Zhu, and Y. Ma, Phys. Rev. B **82**, 094116 (2010).
[3] L. Zhu, H. Liu, C. J. Pickard, G. Zou, and Y. Ma, Nat. Chem. **6**, 644 (2014).
[4] M. Zhang, H. Liu, Q. Li, B. Gao, Y. Wang, H. Li, C. Chen, and Y. Ma, Phys. Rev. Lett. **114**, 015502 (2015).
[5] L.-C. Xu, R.-Z. Wang, M.-S. Miao, X.-L. Wei, Y.-P. Chen, H. Yan, W.-M. Lau, L.-M. Liu, and Y.-M. Ma, Nanoscale **6**, 1113 (2014).
[6] Z. F. Wang, N. Su, and F. Liu, Nano Lett. **13**, 2842 (2013).
[7] X. Luo, J. Yang, H. Liu, X. Wu, Y. Wang, Y. Ma, S.-H. Wei, X. Gong, and H. Xiang, J. Am. Chem. Soc. **133**, 16285 (2011).
[8] W. Luo, Y. Ma, X. Gong, and H. Xiang, J. Am. Chem. Soc. **136**, 15992 (2014).
[9] G. Kresse and J. Furthmüller, Phys. Rev. B **54**, 11169 (1996).
[10] J. P. Perdew, K. Burke, and M. Ernzerhof, Phys. Rev. Lett. **77**, 3865 (1996).
[11] G. Kresse and J. Furthmüller, Comput. Mater. Sci. **6**, 15 (1996).
[12] S. Grimme, J. Comput. Chem. **27**, 1787 (2006).
[13] J. Heyd, G. E. Scuseria, and M. Ernzerhof, J. Chem. Phys. **118**, 8207 (2003).
[14] K. Parlinski, Z. Q. Li, and Y. Kawazoe, Phys. Rev. Lett. **78**, 4063 (1997).
[15] A. Togo, F. Oba, and I. Tanaka, Phys. Rev. B **78**, 134106 (2008).
[16] X. Gonze and C. Lee, Phys. Rev. B **55**, 10355 (1997).